Research Article

Saman Rashid, Muhammad Khurram Waqas, Ayesha Tahir, Haya Yasin*, Bushra Nasir*, Abida Kalsoom Khan, Munaza Ijaz, and Ghulam Murtaza*

Fabrication of antibacterial chitosan/PVA nanofibers co-loaded with curcumin and cefadroxil for wound healing

https://doi.org/10.1515/gps-2025-0010
received November 08, 2024; accepted March 29, 2025

Abstract: This study aimed to prepare chitosan/PVA nanofibers loaded with cefadroxil and curcumin (CPCCNFs) by electrospinning. According to FTIR spectra, there was no interaction between drugs and polymers. X-ray diffractograms showed the amorphous nature of cefadroxil and curcumin in its nanofiber form. According to thermogravimetric analysis results, CPCCNFs remained thermally stable up to 423°C. CPCCNFs exhibited an initial swelling ratio of 80.76% and an erosion rate of 44.2%, indicating a good liquid absorption capacity. Dissolution tests showed an initial burst release of 75% of the drug within the first hour, followed by the sustained release over 2 h. The zeta potential of CPCCNFs ranged from −9.6 to +11.1 mV, confirming good colloidal stability. The antibacterial results showed an appreciable zone of inhibition of 14.6 ± 1.0 mm against *Staphylococcus aureus*, demonstrating the strong antibacterial potential of CPCCNFs. According to wound closure and histopathological studies, CPCCNF-treated wounds exhibited a 60% reduction by day 3, 72% by day 7, 85% by day 14, and complete closure by day 19, significantly outperforming the positive control (Quench) and negative control (untreated). The characterizations confirmed the successful synthesis of stable CPCCNFs with good antibacterial potential against Gram-positive bacteria and a promising wound healing ability.

Keywords: electrospinning, *Staphylococcus aureus*, swelling ratio, combination therapy, skin regeneration

*** Corresponding author: Haya Yasin,** Department of Pharmaceutical Sciences, College of Pharmacy and Health Sciences, Ajman University, 346, Ajman, United Arab Emirates, e-mail: haya.yasin@gmail.com, tel: 00923142082826, fax: 00924299204787
*** Corresponding author: Bushra Nasir,** Department of Pharmaceutics, Faculty of Pharmacy, Bahauddin Zakariya University, Multan, Pakistan, e-mail: bushranasirbzu@gmail.com
*** Corresponding author: Ghulam Murtaza,** Department of Pharmacy, COMSATS University Islamabad, Lahore Campus, Lahore, Pakistan, e-mail: gmdogar356@gmail.com
Saman Rashid: Department of Pharmaceutics, Faculty of Pharmacy, Bahauddin Zakariya University, Multan, Pakistan
Muhammad Khurram Waqas, Ayesha Tahir: Institute of Pharmaceutical Sciences, University of Veterinary & Animal Sciences, Lahore, Pakistan
Abida Kalsoom Khan: Department of Chemistry, COMSATS University Islamabad, Abbottabad Campus, Abbottabad, Pakistan
Munaza Ijaz: Department of Microbiology, University of Central Punjab, Lahore, 54000, Pakistan

1 Introduction

Skin is the largest organ of the body and serves as a protective barrier against injurious substances in the surrounding environment and is susceptible to burn, surgery, and accidents [1]. The healing phenomenon begins when the skin loses its integrity [2]. Wound healing comprises inflammation, proliferation, and remodeling phases. Traditional wound dressings provide insulation and hemostatic properties [3] but can lead to overhydration and wound infection [4]. The moist environment plays an important role in the remodeling of the blemish area allowing migration of epithelial cells from the circumferences of the wound bed [5].

Advanced wound dressings accelerate angiogenesis [6], allow an exchange of gases between wound tissue and the environment, and enhance blood flow by maintaining the temperature of the tissues [7]. Allografts and xenografts are skin-restoring procedures, called skin substitutes, and improve the regeneration of tissues in severe skin burn instances [8]. These techniques refer to the relocation of healthy skin to the wound area along with risks of transmission of disease and the body's immune responses [9]. A restricted supply of fresh allografts is also the main concern in these techniques [10].

Biodegradable and biocompatible polymers such as pectin and chitosan are now being used as a supply system of different active pharmaceutical ingredients with no obvious side effects. Polymer-based wound dressings loaded

with bioactive components have exhibited considerable promise for antibacterial and regenerative features [11,12]. Nanofibers with a diameter of nanometer range have promising properties [13] like porosity, elasticity, large surface area, and biodegradability in a cascade of wound healing [14]. Water-soluble synthetic polymer PVA derived from vinyl acetate has been used in the nanocomposite film owing to its hydrophilicity, low toxicity, high absorption of exudates, elasticity, and biocompatibility properties [15]. Chitosan is a biodegradable and thermal-resistant polymer with antibacterial and mucoadhesive properties and enhances the adhesion of cells and differentiation in the regeneration of tissues without any immune responses in all phases of the healing process [16].

Cefadroxil is a broad-spectrum antibiotic of first-generation cephalosporin and is effective against Gram-positive bacteria, especially *Staphylococcus aureus* used in infections of the respiratory tract, skin, and urinary tract [17]. Curcumin, the active component of turmeric, can scavenge radicals [18,19] that hinder the healing process along with anti-inflammatory properties [20]. It has a competency to increase the regeneration of epithelial cells and the proliferation of fibroblasts in the healing of wounds [21,22].

Nanoparticles of curcumin facilitated the increased cellular uptake of curcumin as compared to its raw form with an extended half-life [23]. Chitosan and sepiolite-based nanocomposite films were formulated against *B. subtilis* and *E. coli* for effectual wound healing [24]. Zhang et al. eminently made CS/PVP/DHQ nanocomposite dressings with antimicrobial and antioxidant properties with no distinct toxic effect on haCat keratinocytes [14]. Govindasamy et al. successfully prepared ZnO/CuO-based nanocomposite film against Gram-positive *S. epidermidis* with a greater degradation rate in 8 days as compared to commercially available products [25]. Hydrogel accommodating photothermal silver nanoparticles with hyaluronic acid-tyramine was put together by Chang et al. to accelerate wound healing that was dually infected with *S. aureus* and *E. coli*. After 2 weeks, the wound healing ratio in the HT and HTA groups was greater than in the control group [26]. Wang et al. formulated sodium alginate/polyvinyl alcohol/taxifolin-based nanofibers to enhance wound amelioration in foot ulcers in diabetic patients with a release profile of 64.6 ± 3.7% at 24 h [27]. Kamalipooya et al. prepared mates of PCL/CA/CeO2-CSNP nanofiber that showed excellent anti-oxidant activity in wound care against *S. aureus* with a clear zone of inhibition of 17 mm as compared to the control disk of vancomycin with 10 mm [28]. Wang et al. enacted a diversified nanofibrous dressing. Angiogenesis was accelerated by the addition of strontium ions into the PLCL nanofilm, followed by the subsequent addition of PDA and ZnO. The photothermal and non-drug anti-microbial effect of PDA was observed in the elimination of *S. aureus* and *E. coli* in wound healing [29]. The combination of cefadroxil and chitosan in *in situ* gel was managed by Basha et al. with the purpose of penetration in different strata of the skin for wound remedy [30]. Nanofibers with chitosan are fragile and prone to destabilization. Iqbal et al. formulated nanofibers of cefadroxil-loaded chitosan and PVA against clinical isolates *S. aureus* with improved mechanical strength [31,32].

This study aimed to formulate cefadroxil and curcumin-loaded nanofibers with biodegradable and biocompatible polymers (chitosan and PVA) for the effective healing of wounds infected with *S. aureus* through an electrospinning technique. While several studies have explored dual-drug nanofiber systems, they typically involve different antibiotic and bioactive agent combinations. For example, Basha et al. developed an *in situ* gel-based system of cefadroxil-loaded chitosan nanoparticles for wound healing, but it lacked the structural advantages of nanofibers for sustained release and enhanced mechanical properties [30]. Similarly, Rezagholizade-Shirvan et al. formulated curcumin-loaded chitosan–PVA–alginate nanocomposites, but these lacked the antibacterial efficacy of a potent β-lactam antibiotic [41]. In contrast, our study uniquely combines cefadroxil, a broad-spectrum cephalosporin antibiotic, with curcumin, a natural anti-inflammatory, and antioxidant, in a nanofiber matrix to achieve synergistic antibacterial and wound healing effects. To increase the nanofiber's mechanical properties, montmorillonite (MMT) was used. Although a formal Design of Experiments was not used, this study was conducted systematically to assess the impact of major variables, including polymer composition, drug quantity, and electrospinning variables. This systematic methodology confirmed the reliability and reproducibility of the findings, suggesting the development of CPCCNFs with optimal features for wound healing uses.

2 Experimental method

2.1 Materials

Chitosan (average acetylation 75–86%, MW range 50,000–190,000 g·mol^{-1}), polyvinyl alcohol (PVA, M_W 146–186 kDa), montmorillonite (MMT), nutrient agar (NA), Muller–Hinton agar (MHA), Muller–Hinton broth (MHB), and Dulbecco's modified Eagle's medium (DMEM) were purchased from Sigma-Aldrich (International Laboratory, USA). Cefadroxil (Mol. Wt. 363 and 100% claimed purity) was acquired as a gift from Saffron Pharmaceuticals (Pvt) Ltd (Islamabad, Pakistan). Solvents of the analytical category were

purchased by native vendors. The clinically isolated strain of *S. aureus* was collected from the burn unit of Jinnah Hospital Lahore, Pakistan.

2.2 Solution preparation

Chitosan solution (w/w) was prepared by dissolving 1.7 g of chitosan in distilled water (12 ml) containing a few drops of dilute acetic acid solution (1% v/v) by stirring at 340 rpm at 50°C for about 2 h. On the other hand, 1.7 g of PVA was dissolved in distilled water (12 ml) to prepare the PVA solution (w/w) by stirring at 340 rpm at 50°C for about 12 h. The chitosan solution was added in drops to the PVA solution by continuous stirring for 30 min at 340 rpm speed and standard room temperature (25 ± 2°C). Both solutions were used in equal volumes to ensure a 1:1 ratio between the quantities of polymers.

The solutions of both drugs (cefadroxil and curcumin) were separately prepared by dissolving 0.05, 0.1, 0.15, and 0.2 g of each drug in 2 ml of distilled water and methanol, respectively. The total drug content was 0.2 g. These solubilized drug solutions and 1% MMT were added to a polymeric mixture with continued stirring for about 10 h before their conversion into nanofibers while maintaining the temperature of the polymeric mixture at 40°C. Blank nanofibers contained no drug and were thus used as a control (Table 1).

2.3 Development of drug-loaded nanocomposite solution

Electrospinning was conducted under controlled conditions to ensure the uniformity in the fabricated nanofiber's diameter. The electrospinning approach employed in this study, extensively used in developing nanofibers for biomedical applications, was optimized, as reported by Ghosal et al. [36] in their fabrication of electrospun curcumin–chitosan mats for wound management. The electrospinning approach employed in this study, extensively used in developing nanofibers for biomedical applications, was optimized based on systematic variations in voltage, flow rate, and needle-to-collector distance, similar to the method reported by Ghosal et al. [36]. The formulated solution was loaded in a 5 ml syringe (exhibiting 12 mm diameter) fitted with a polystyrene microtip affixed to a steel nozzle. The nozzle of the FLUIDNA TEK-LE-10 electrospinning machine was fastened to a high-voltage electrical supply of 17 kV, and spinning was executed at a feeding momentum of 0.3–0.6 $ml{\cdot}h^{-1}$. A constant distance of 14 cm was maintained between the needle tip and the grounded aluminum collector. The relative humidity and temperature were in the range of 35% and 20–25°C, respectively. For the folding of the fabricated nanofibers, an iron drum was whirled by a DC motor at abiding speed. A static collector plate covered with aluminum foil was used to deposit the fibers. Water and methanol were allowed to evaporate in an open atmosphere. They fabricated nanofibers were then air-dried overnight and kept in a desiccator for further use. The formulation table representing the formulation pattern of nanofibers is given in Table 1.

2.4 Chemical characterization

2.4.1 Scanning electron microscopy (SEM)

The 3D structure of the film was examined using a Joel JSM 6400 F scanning electron microscope. It involves the application of intense radiation on a sample to produce a variety of signals that will provide surface characteristics [33].

2.4.2 Fourier transform infrared (FTIR) spectroscopy

FT/IR-6600 type A in a 500–4,000 cm scanning range was used to analyze the functional groups, intermolecular

Table 1: Composition of different formulations due to varied quantities of cefadroxil and curcumin

Formulation nanofiber	Chitosan (g)	PVA (g)	MMT (%)	Cefadroxil (g)	Curcumin (g)
A1	1.7	1.7	1	0	0
A2	1.7	1.7	1	0.2	0
A3	1.7	1.7	1	0	0.2
A4	1.7	1.7	1	0.1	0.1
A5	1.7	1.7	1	0.15	0.05
A6	1.7	1.7	1	0.05	0.15

interactions, and nature of bonding in the sample. Infrared radiation induces vibrational transitions in a sample, and the spectrum is recorded when the frequency of the absorbed radiation coincides with the natural frequency of the bond [13].

2.4.3 X-ray diffraction (XRD) spectroscopy

Solid structural analysis was used to differentiate between the crystalline and amorphous forms of nanofibers by XRD spectroscopy [4].

2.4.4 Thermogravimetric analysis (TGA)

A thermogravimetric analyzer (DTG-60H, Shimadzu, Japan) was used to check the thermal integrity of the sample. The sample was kept in an analysis chamber with a constant flow rate of 20 ml·min^{-1} of nitrogen. The temperature was raised to 500°C at a rate of 10°C·min^{-1} after precise weighing.

2.4.5 Zeta size and zeta potential

The zeta size and zeta potential of all film formulations were evaluated by a Zeta sizer with a minimum of 3.8 nm and a maximum of 100 µm size. Readings were listed at 25°C, and standard deviation was estimated.

2.5 Pharmaceutical research

2.5.1 Swelling ratio

The swelling ratio study was accomplished by immersing the pre-weighed films in a freshly prepared phosphate buffer solution. At a predetermined period (10, 20, 30, 60 min, 1.5, 2, 3, 4, 6, 8, 12, 16, 20, and 24 h), each film was withdrawn from the solution and placed back after weighing. The excess surface water of the film was removed by filter paper and subsequently weighed through an electronic weighing balance [13]. The swelling ratio was examined by the following equation:

$$\mathrm{SR} = W_h/W_d$$

where W_h is the weight of the swollen film, and W_d is the weight of the dry film.

To determine the percentage increase in weight, the following equation was used:

$$\text{Water content (\%)} = W_h - W_d/W_h\ (100)$$

where W_h is the mass of the swollen film at time t, and W_d is the primary mass of the dry film.

2.5.2 Erosion study

Gravimetric or equilibrium techniques were used to conduct erosion studies. Owing to water uptake experiments, the wet films were dried for 12 h at 40°C in an oven and then subsequently cooled in desiccators. The films were weighed at regular intervals. Each experiment was performed in triplicate [8]. The equation used to calculate film erosion is as follows:

$$\text{Film erosion (\%)} = (W^\circ - W_f/W^\circ)\ 100$$

where W_f is the overall weight of the dry films, and W° is the initial weight of the swollen films.

2.5.3 Porosity of nanofibers

To identify the voids in the nanofiber matrix, porosity was calculated using a scanning electron microscope analyzer. The volume difference between the dipped sample and displaced liquid volume was calculated [11]. The formula used to find the porosity of CPCCNFs is as follows:

$$\text{Porosity (\%)} = W_2 - W_1/\rho V_1 - \rho V_2\ (100)$$

where W_2 is the weight of the wet sample, W_1 is the weight of the dry film, V_1 is the volume of the solvent before adding the nanofiber, and V_2 is the volume of the solvent after removing the nanofiber.

2.5.4 Calibration curve development

A phosphate buffer solution (1,000 ml) was prepared by dissolving 6.8 g of potassium phosphate monobasic in distilled water [34]. Potassium hydroxide was used to adjust the pH to 6.8. The buffer solution was sonicated for 10 min. A mixture of phosphate buffer and acetonitrile (96:4) was filtered and degassed. A total of 25 mg of cefadroxil was added to a volumetric flask containing 12.5 ml of phosphate buffer solution and the volume was made up to 25 ml. The solution in the flask was sonicated for 15 min. Then, 50 µg·ml^{-1} (stock solution) was formed by diluting the 5 ml solution of flask up to 25 ml in the mobile phase. Subsequently, a further five test dilutions were made from the stock solution. All solutions were pre-filtered before the sample was added to the column. At last, the calibration curve was drawn, and readings were taken thrice.

2.5.5 Drug content uniformity

To check the drug content uniformity of the film taken from the center and proximity, the film was placed in a 100 ml volumetric flask containing phosphate buffer. The flask was sealed and agitated overnight by using a magnetic stirrer to check the release rate of medication from the films. The mixture was divided into aliquots, each in a range of 50 mg·ml^{-1}, filtered through Whatman-41 filter paper, and then reconstituted. A UV-visible spectrophotometer (O.R. 13000, UV-VIS Spectrophotometer, Germany) was used to measure the absorbance at 254 nm to estimate the drug content [25].

2.5.6 Drug release study

A drug release study was conducted using Dissolution apparatus I (Basket method). Nanofibers were bound to the basket to prevent its floating in the dissolution medium. The temperature of the dissolution medium PBS was adjusted at 37 ± 0.5°C and 50 rpm. The film samples were cut and placed in a glass vial containing 300 ml of phosphate buffer solution. At fixed periods of 15, 30, 45, and 60 min, aliquots of 5 ml were drawn and replaced by an equivalent volume of fresh phosphate buffer solution to maintain a constant volume throughout the procedure. A UV spectrophotometer (Shimadzu, UV-1280) was used to examine the drug release at 233 nm [19]. The study was conducted in triplicate. Dissolution data were further assessed through kinetic models, using zero order, first order, and Higuchi equations [4]. The dissolution data best fit the first-order model (R^2 = 0.984), indicating concentration-dependent drug release. The amorphous state of cefadroxil and curcumin, confirmed by XRD, contributed to faster dissolution due to higher molecular dispersion within the nanofiber matrix.

2.5.7 *In vivo* evaluation of nanofibers

An animal study was conducted to evaluate and compare the wound healing effect of CPCCNFs with conventional Quench cream. The experiment was performed on four male rabbits, each of 2–3 kg. The rabbits were labeled as control, standard, drug-loaded, and without drug-loaded. Xylene (15 mg·kg^{-1}) and ketamine HCl (75 mg·kg^{-1}) were used to induce anesthesia in rabbits. The dorsal region of rabbits was shaved and cleaned with 75% ethanol to minimize the risk of sepsis. A sterile biopsy punch made incisions, each of 3 cm^2 in the area and half a centimeter in thickness. One incision was affected with bacterial strains while leaving the other uninfected. The rabbit labeled as control was left untreated, while on the second and third, electrospun CPCCNFs and NFs without curcumin and cefadroxil were applied. On standard rabbits, the marketed product Quench cream was used. The experimental conditions were constant for all the rabbits. The diameter of the wound was measured on the first day of development. All set formulations were applied daily on rabbits' wounds for 21 days. During the experiment, the rabbits were served with carrots and herbs. Daily measurements were taken and compared with control and standard. To calculate the wound's width, the following formula was used:

$$\text{Wound area (\%)} = (A/A^\circ)\,100$$

where A° is the initial wound area, and A is the wound area after a set time.

2.5.8 Antimicrobial assay

The antimicrobial activity of electrospun CPCCNFs was examined by the disc diffusion method against *S. aureus*. Nutrient agar media was prepared by dissolving 0.0896 g of nutrient agar in 40 ml of distilled water. Petri plates and nutrient agar media were autoclaved for 2.5 h at 121°C. Afterward, the sterilized media was poured into the Petri plates in a laminar flow hood and allowed to settle at room temperature. A loopful of *S. aureus* strain was uniformly spread on nutrient agar and incubated for 24 h at 37°C. After this, each film with 10 mm × 10 mm dimensions was placed on inoculated media and incubated at 37°C for 48 h. After the incubation period, the zone of inhibition was measured (in mm) to determine the antimicrobial activity of the formed films [29].

2.5.9 Histopathological investigation

The wound sites were taken out, and the histopathological impact of the CPCCNFs was examined. The biopsies of skin were embedded in paraffin and then fixed with 10% formalin. Glass slide paraffin sections were cut and stained with hematoxylin and eosin. The histopathological changes were evaluated and photographed by a light microscope equipped with a camera [7].

2.6 Statistical evaluation

Mean and standard deviation were calculated using SPSS 20.0. One-way ANOVA was used to determine the

significance of differences. p values less than 0.05 were considered significantly different.

2.7 Ethical approval

The research related to animal use has been complied with all the relevant national regulations and institutional policies for the care and use of animals. For the *in vivo* study of drug-loaded electrospun NFs, the protocol used was accepted by the Research Ethics Committee with approval no. M4/23-897 for the continuum care and use of laboratory animals from the Department of Pharmacy (COMSATS University, Islamabad Lahore Campus, Pakistan). All animal experiments comply with the ARRIVE guidelines and were carried out following the National Institutes of Health guide for the care and use of Laboratory animals (NIH Publications No. 8023, revised 1978).

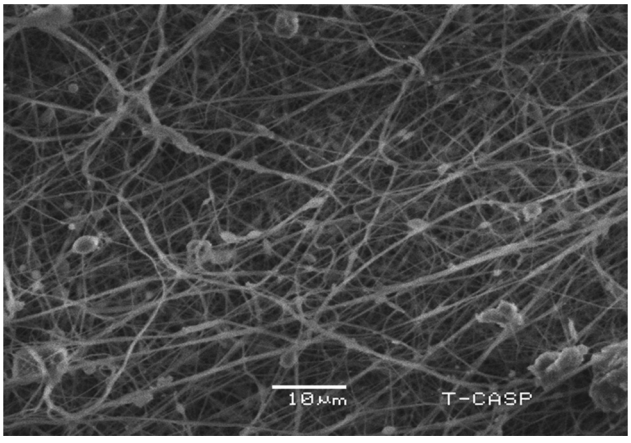

Figure 1: SEM micrographs of A4 formulation with a scale bar of 10 µm. The uniform fiber distribution and bead-free morphology confirm the successful electrospinning of CPCCNFs.

3 Results and discussion

3.1 Chemical characterization of nanofibers

3.1.1 Scanning electron microscopy (SEM)

SEM analysis revealed that the A4 formulation had a smooth surface and was amorphous, similar to nanofiber-based wound dressings reported by Ghosal et al. [35], where the addition of bioactive agents modified fiber morphology without compromising uniformity. The presence of small beads observed in our study aligns with findings in electrospun curcumin–chitosan mats, where viscosity-dependent fiber formation affected entrapment and release kinetics [35]. This further supports the role of polymeric interactions in determining the nanofiber structure. Figure 1 shows the even distribution of Cefadroxil. Pandey et al. explained similar changes in the morphology of nanofibers due to the addition of curcumin [36]. Chitosan can increase the elongation force of the film along with modification in the viscosity of the blend and surface charge density [37].

3.1.2 FTIR spectroscopy

The FTIR spectra of drug-free nanofibers and CPCCNFs are shown in Figure 2. The FTIR spectra indicated the type of interaction between the polymer and drug functional groups of CPCCNFs [37]. The FTIR spectra of CPCCNFs showed

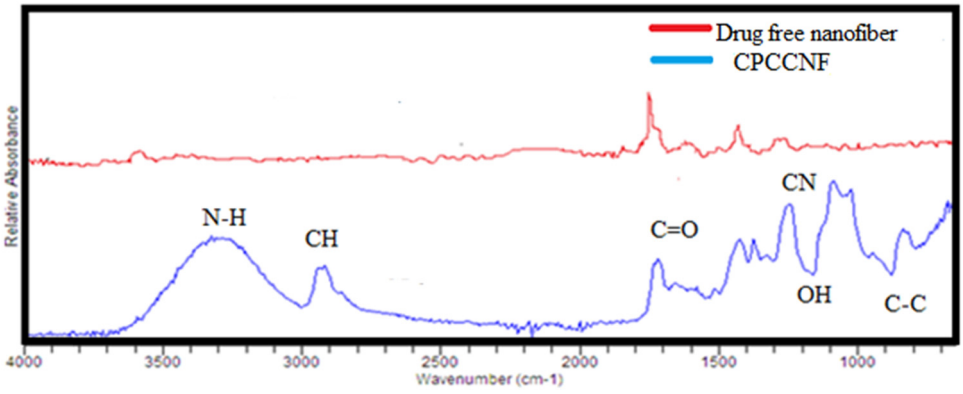

Figure 2: FTIR spectra of drug-free NFs and CPCCNFs, with major peaks for NH (3,300 cm^{-1}), CH (2,920 cm^{-1}), C═O (1,705 cm^{-1}), and OH (1,150 cm^{-1}).

different peaks at different wavelengths, i.e., the NH bond peak at 3,300 cm^{-1}, the CH bond peak at 2,920 cm^{-1}, C═O bond peak at 1,705 cm^{-1}, C–N bond peak at 1,220 cm^{-1}, OH bond peak at 1,150 cm^{-1}, and C–C bond peak at 890 cm^{-1}. A broad peak indicates the presence of OH groups and CH groups and stretching. Other peaks are due to the presence of the CO, CN, and NH groups. The FTIR spectra of drug-loaded CPCCNF nanofibers did not reveal any new peaks, indicating that their functional groups did not interact [38].

FTIR analysis confirmed the absence of significant chemical interactions between the polymers (chitosan and PVA) and the drugs (cefadroxil and curcumin), as indicated by the retention of characteristic peaks for all components. To provide a clearer understanding of the structural and functional arrangement within the CPCCNFs, a schematic representation is shown in Figure 3. This schematic illustrates the encapsulation of cefadroxil and curcumin within the nanofiber matrix and highlights the key functional groups involved in hydrogen bonding between the polymer chains. The interactions ensure the stability of the nanofibers while maintaining the independent functionalities of the drugs, as supported by FTIR spectra. Moreover, the physical characteristics observed in SEM analysis, such as smooth surface morphology and porosity, complement the chemical stability suggested by the FTIR spectra. Together, these findings confirm that the CPCCNFs are well-suited for drug delivery applications and provide a foundation for effective wound healing.

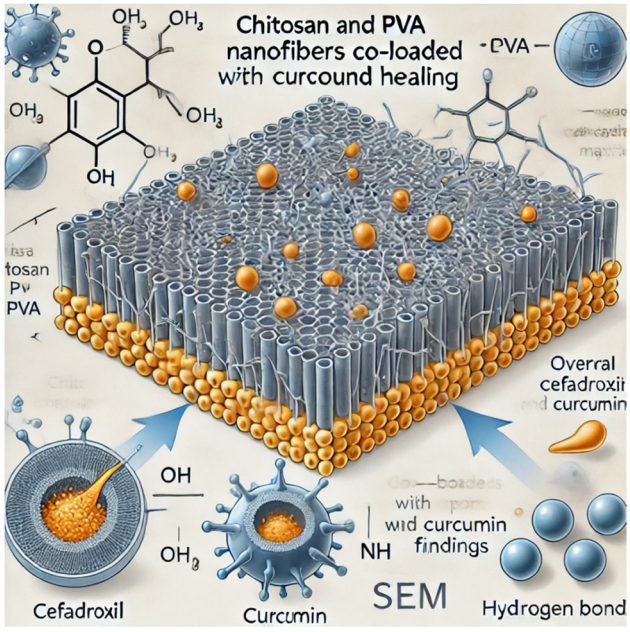

Figure 3: Illustrative representation of the chemical and physical association within CPCCNFs. The diagram indicates the role of chitosan and PVA as a polymeric matrix, the encapsulation of cefadroxil and curcumin, and the linkage between functional groups, as confirmed by FTIR analysis.

3.1.3 XRD spectroscopy

The diffractograms of cefadroxil, curcumin, and CPCCNF (Figure 4) display diffraction peaks in their XRD patterns at 15° and 18° and a single broad peak at 2θ = 15°, the Bragg angle. The amorphous nature and stretched molecular chain at high elongation of the nanofibers resulted in the widening of the peak. The drug's diffractogram contained sharp and intense diffraction peaks, especially in the range of 10°–30° (2θ), suggestive of its crystalline feature. These peaks exhibit the ordered arrangement of molecules in the pure drug form, showing their intrinsic crystalline structure. In contrast, the XRD pattern of CPCCNFs indicates a broad halo with the absence of sharp peaks, especially between 10° and 30°, which is a feature of the amorphous substance. The broadening of peaks and the diminished intensity in CPCCNFs indicate that cefadroxil and curcumin are molecularly dispersed within the polymeric nanofiber matrix, resulting in the loss of crystallinity. These amorphous features improve the solubility and dissolution rate of the added drugs, which is useful for drug release. Moreover, the lack of specific peaks for curcumin in the nanofiber composite further ensures its successful addition and dispersion within the amorphous polymer structure. The change from crystalline to amorphous form reveals the usefulness of the electrospinning process in producing homogeneously distributed drug-loaded nanofibers. Massoumi et al. explained that curcumin can increase lattice parameters and decrease the crystallinity of the sample [39].

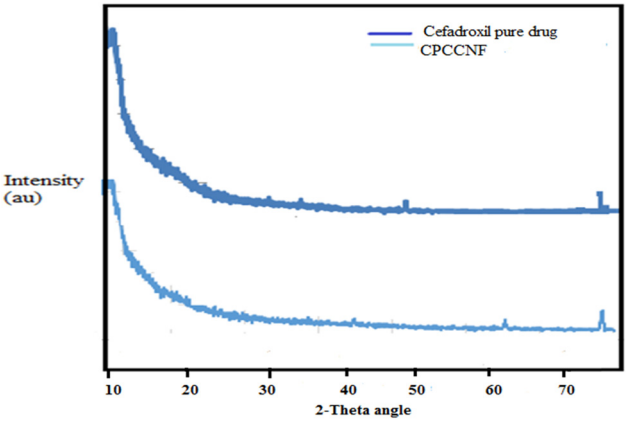

Figure 4: XRD patterns of CPCCNFs and pure cefadroxil with typical diffraction peaks confirming the amorphous nature of CPCCNFs.

Nanoparticles of cefadroxil and chitosan *in situ* gel exhibited the amorphous nature of the sample and loss of crystallinity due to encapsulation of the drug in the formed nanoparticles [30].

3.1.4 TGA

The TGA graph of the A4 formulation revealed the stability and weight loss due to moisture evaporation at different temperatures. When heat flows at 115°C, 10–15% weight loss was observed. At 300°C, the breakdown of the polymers, chitosan/PVA, started. At 423°C, the breakdown of the whole matrix occurred. The TGA thermogram of the composite system (Figure 5) reveals thermal stability and decomposition behavior. The initial weight loss observed below 100°C, responsible for about 20% of the weight, corresponds to the evaporation of moisture and loosely bound water molecules from the polymer matrix. This is typical for water-soluble substances such as chitosan and PVA, which can preserve adsorbed water. A second weight loss, observed between 100°C and 250°C, indicates the removal of volatile substances and partial decomposition of low-molecular-weight ingredients, including any residual solvents or volatile byproducts from the drug–polymer interaction. The primary and most considerable weight loss event, initiating from about 250°C and extending to 400°C, reveals the thermal degradation of the main polymer backbone along with encapsulated drugs. This step involves the degradation of chitosan, PVA, and drug molecules, leading to a major mass loss of about 30%. Beyond 400°C, the remaining weight stabilizes, signifying the development of carbonaceous residues and stable char, with no significant further mass loss. The associated heat flow curve indicates an exothermic event related to the major decomposition phase, suggesting the thermal degradation processes. This thermal profile emphasizes the composite's thermal feature, reflecting its stability for drug delivery use within the expected temperature ranges for storage and processing. The addition of fillers did not affect the stability of chitosan/PVA-based nanofibers analyzed by TGA [40]. PVA and curcumin can increase the thermal stability of the formulation [30]. Iqbal et al. observed that cefadroxil-loaded chitosan/poly(vinyl alcohol) nanofibers were more heat-stable than nanofibers free from cefadroxil [38].

3.1.5 Zeta size and zeta potential

For a formulation to be stable, zeta size and zeta potential should be within the acceptable range.

The average zeta size of <200 nm and zeta potential of −9.3 mV to +9.1 mV were observed for CPCCNFs. The more the positive values, the higher the particle stability. Both values of all the formed formulations were different due to varying concentrations of drugs and polymers and molecular charge and ionic strength of the solution. The zeta potential of formulations was in the order of A3 > A5 > A6 > A4 > A1 > A2 and order of zeta size was A4 > A3 > A5 > A1 >

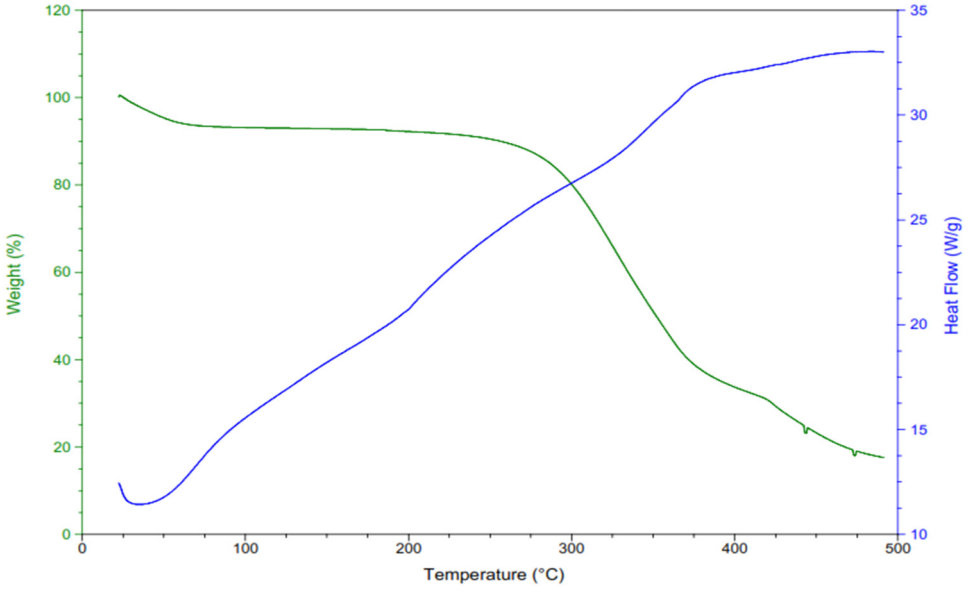

Figure 5: TGA graph of A4 formulation.

A6 > A2. The negative value of the zeta potential of A2 showed the weak van der Waal's forces between the drugs and solution. Similarly, the A4 formulation exhibited higher particle size, indicating its higher stability. All prepared formulations are significantly ($p < 0.05$) different. The zeta size and zeta potential were measured to assess colloidal stability before electrospinning. The zeta potential ranged from −9.6 mV to +11.1 mV, with A3 exhibiting the highest value (+11.1 mV), indicating better electrostatic repulsion and reduced aggregation. Higher zeta potential values contributed to improved jet stability and smoother nanofiber morphology, while formulations with lower zeta potential (e.g., A2: −9.6 mV) showed occasional fiber bead formation due to weak electrostatic forces. These findings align with previous studies, demonstrating that higher surface charge enhances uniform fiber formation by preventing premature jet breakup. Future studies could further optimize solution charge dynamics to improve nanofiber consistency. Kumar and Kaur observed that the particle size would be higher if the concentration of the biomolecules were increased. In contrast, the zeta potential of biomolecules acted as a capping agent and stabilized the nanofilms by creating steric hindrance [34]. Table 2 represents the zeta analysis results for formulations.

3.2 Pharmaceutical research

3.2.1 Swelling ratio

The swelling ratio of all CPCCNFs was observed in PBS, as shown in Figure 6. Chitosan/PVA polymers have maximum solvent absorption capacity due to the availability of an increased number of hydrophilic groups. Hence, drug-free nanofibers A1 showed more solvent absorption than CPCCNFs in the initial 15 min and were significantly different ($p < 0.05$). Drug-based nanofibers exhibited lesser solvent absorption due to the hydrogen bonding between drug and polymers and a decrease in the number of free

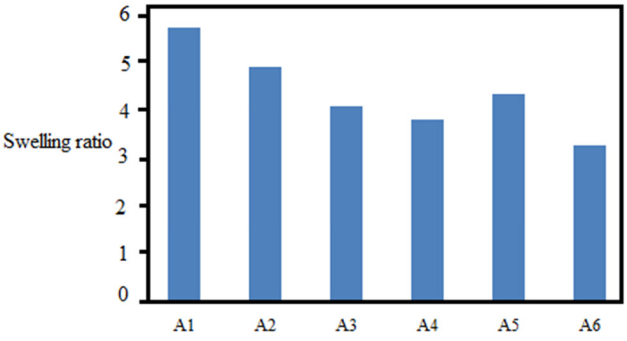

Figure 6: Swelling ratios of different CPCCNF formulations.

OH groups. After 1 h, the swelling index of each CPCCNF was decreased due to the deterioration of the polymers. The decreasing order of CPCCNF swelling was A1 > A2 > A5 > A3 > A4 > A6. In CPCCNFs A2 and A5, preparations showed an increased swelling ratio owing to the increased content of water-soluble cefadroxil than that in curcumin. The experiment was performed in triplicate.

3.2.2 Erosion study

The gravimetric method was used to determine the percentage of erosion in CPCCNFs, as shown in Table 3. The ability to absorb solvent is directly related to the erosion phenomenon. Films with higher absorption capacity exhibited a higher erosion rate [9]. As the A1 formulation was free of drug, it showed higher erosion due to increased solvent uptake. The order of erosion of CPCCNFs was A1 > A2 > A5 > A3 > A4 > A6. In the drug base nanofibers, A2 and A5 exhibited faster erosion rates due to the increased amount of water-miscible drug cefadroxil. Formulations with higher swelling (A2: 79.75%) and erosion (A2: 40.5%) exhibited faster drug release (80% in 1 h), correlating with enhanced antibacterial efficacy (14.6 mm inhibition zone) and faster wound closure (85% by day 14). These findings confirm that liquid absorption capacity influences drug diffusion and therapeutic outcomes.

Table 2: Zeta analysis of all formulations

Formulations	Zeta size (nm) ± SD	Zeta potential (mV) ± SD
A1	182.1 ± 1.8	2.9 ± 0.01
A2	135.7 ± 1.1	−9.6 ± 0.2
A3	733 ± 1.5	11.1 ± 0.2
A4	1291 ± 2.8	3.9 ± 0.1
A5	482.1 ± 1.8	6.8 ± 0.1
A6	145.0 ± 0.2	6.2 ± 0.1

Table 3: Erosion (mean ± SD) of all formulations

Formulations	Erosion (%) (mean ± SD)
A1	44.1 ± 0.62
A2	40.5 ± 0.92
A3	34.1 ± 0.30
A4	32.1 ± 1.15
A5	39.7 ± 0.27
A6	29.9 ± 0.47

3.2.3 Porosity

The SEM analyzer exhibited the porosity (voids) in CPCCNFs, as shown in Table 4. Porosity is directly related to the swelling phenomenon. Figure 6 shows a higher porosity in three formulations of the order A1 > A2 > A5 than the other three in the sequence A3 > A4 > A6. As the drug-free formulation A1 has a greater swelling index, it has a greater porosity than A2 and A5. A3 > A4 > A6 showed lesser porosity owing to increased curcumin (hydrophobic) content than cefadroxil. Porosity allows the continuous release of drugs from the nanofiber films unveiling the positive effects in wound healing [21].

3.2.4 Calibration curve development and drug content uniformity testing

The calibration curve was plotted using various concentrations in triplicate. According to the equation $y = mx + b$, by substituting the value of m (0.033) and b (0.004), the value of R^2 was found to be 0.9941.

The drug contents in all CPCCNF formulations were evenly distributed along the matrix, as displayed in Table 5. Formulation A2 exhibited a greater loading efficiency of 93.839 ± 0.66. No significant differences were observed in the distribution of drug content in the periphery and center.

In addition to drug content uniformity, encapsulation efficiency, and loading capacity were assessed. The encapsulation efficiency (%) ranged from 82.4% to 93.8%, with formulation A2 showing the highest value (93.8 ± 0.66%), while the loading capacity (%) varied between 6.5% and 9.2%. Minor drug loss occurred due to polymer–solvent interactions during electrospinning, but high EE% suggests minimal wastage, ensuring therapeutic efficacy. The retained drug content supports sustained release, enhancing antibacterial and wound healing effects. Future optimizations could further improve drug retention.

Table 4: Porosity (mean ± SD) of all formulations

Formulations	Porosity (%) (mean ± SD)
A1	80.76 ± 0.11
A2	79.75 ± 0.31
A3	49.15 ± 0.04
A4	37.70 ± 0.09
A5	73.34 ± 0.10
A6	24.39 ± 0.08

Table 5: Cefadroxil content uniformity test in all formulations

Formulations	Content in center (% ± SD)	Content in proximity (% ± SD)
A1	90.515 ± 0.22	90.298 ± 0.04
A2	93.839 ± 0.66	93.199 ± 0.125
A3	91.627 ± 0.71	91.535 ± 0.58
A4	93.111 ± 0.73	93.152 ± 0.46
A5	93.602 ± 0.46	93.557 ± 0.56
A6	92.626 ± 0.69	92.456 ± 0.67

3.2.5 Drug release study

The extent of drug release from CPCCNFs was observed through dissolution analysis. The time for the 25% and 50% release of drugs was approximately 6 and 12 min, respectively. The complete release of drugs took about 2 h. The initial 75% release of drugs occurred as a burst, followed by a sustained release. This burst effect has been previously reported in electrospun wound dressings, where hydrophilic polymers such as PVA accelerate initial drug diffusion [35]. Similar release behavior was observed in Ghosal et al., where drug-loaded electrospun mats exhibited rapid initial drug diffusion due to surface-deposited molecules, followed by polymeric matrix-controlled release [35]. In our study, the interaction of chitosan and PVA appears to regulate sustained drug diffusion, ensuring prolonged therapeutic effects. This swift release of drugs could be due to the hydrophilic nature of PVA and drugs. Moreover, kinetic analysis revealed that dissolution data were best explained by the first-order equation. Rezagholizade-Shirvan et al. revealed that a combination of chitosan, polyvinyl alcohol, and alginate allowed the slow release of curcumin, assuring its sustained release from the nanocomposite [41]. The cross-linked network structure of polymers chitosan/PVA allowed the

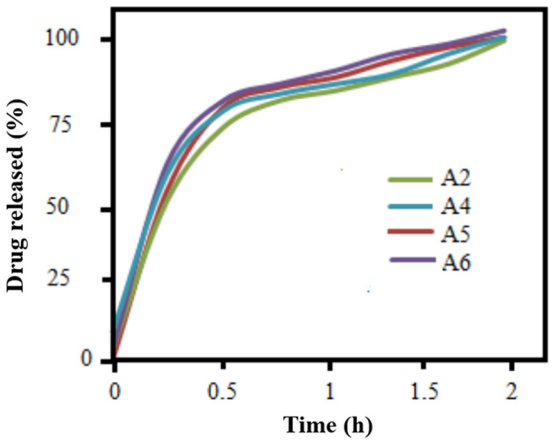

Figure 7: Drug release study of CPCCNFs.

Table 6: Zone of inhibition of all formulations against *S. arogenosa*

Formulations	Zone of inhibition (mm) (mean ± SD)
A1	Nil
A2	14.6 ± 1.0
A3	10.7 ± 1.1
A4	Nil
A5	9.3 ± 0.58
A6	Nil
Standard (cefadroxil)	17 ± 0.70

burst release of the drug in an initial 15–20 min, ensuring the effective delivery system at the start and then sustained release afterward [30]. In this study, A2 formulation showed quick release of the drug cefadroxil due to its higher concentration, loose binding with polymers, and increased solubility in the dissolution medium PBS. This study showed 40% of cefadroxil release in 0.5 h, 80% in 1 h, and complete dissolution in 2 h. The experiment was performed in triplicate. Figure 7 depicts the drug release pattern of all formulations.

3.2.6 Antimicrobial evaluation

The antimicrobial efficacy of various formulations was evaluated against *S. aureus* (Table 6).

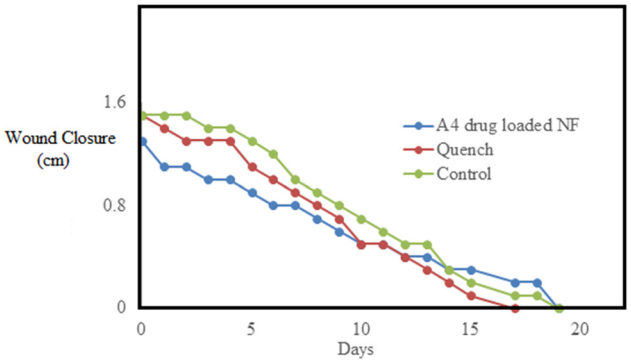

Figure 8: Wound closure comparison of CPCCNF with Quench and control.

The nanofibers exhibited zones of inhibition of 14.6 ± 1.0 mm, 10.7 ± 1.1 mm, and 9.3 ± 0.58 mm, respectively, in decreasing order as A2 > A3 > A5, against standard (17 mm ± 0.70) and were significantly different ($p < 0.05$). However, the nanofibers A1, A4, and A6 did not show a zone of inhibition. CPCCNFs (A4) exhibited a larger inhibition zone (14.6 ± 1.0 mm) than curcumin-only (A3: 10.7 ± 1.1 mm) and cefadroxil-only (A2: 9.3 ± 0.58 mm) nanofibers, indicating an additive antibacterial effect. The observed inhibition zone is comparable to other electrospun nanofiber formulations incorporating antibiotics [12,31]. Ghosal et al. [35] reported

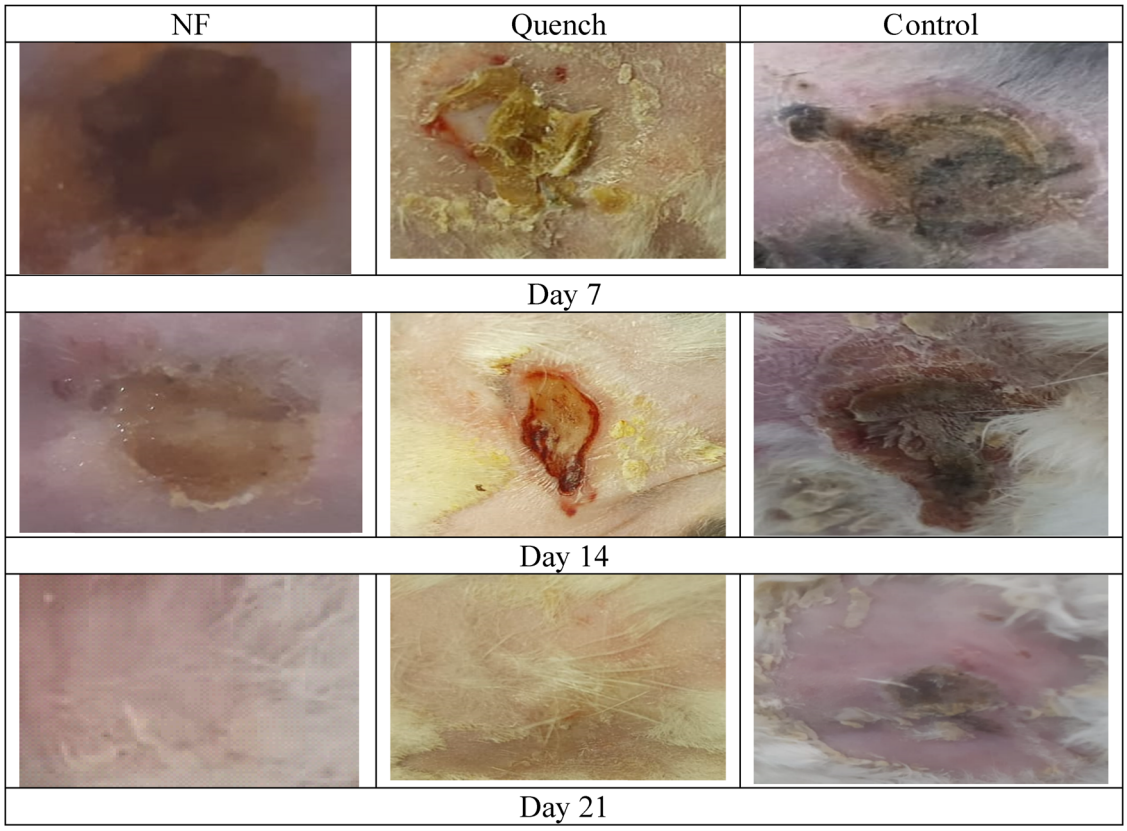

Figure 9: Images of burn wound healing.

that the electrospinning process enhances the surface area, improving the bioavailability and antimicrobial performance of the loaded drugs. Our findings suggest that the synergistic effects of cefadroxil and curcumin further enhance bacterial inhibition, highlighting the potential of CPCCNFs for advanced wound-healing applications.

Antibacterial activity was assessed against *S. aureus* owing to cefadroxil's Gram-positive specificity. While curcumin has reported activity against Gram-negative bacteria like *E. coli* [23], it was not tested here, as the primary focus was on *S. aureus*-dominant wound infections. Future studies will explore its broader antimicrobial potential.

3.2.7 Wound healing

The wound closure rate was observed and compared with the standard (Quench) and untreated models. Figure 8 exhibits the 21-day healing process in rabbits exposed to different formulations. The wound healing rates after the 3rd, 7th, and 14th days were 60%, 72%, and 85%, respectively, and complete closure after the 19th day of treatment with CPCCNFs. CPCCNFs promoted fast wound closure (85% by day 14 and full closure by day 19), confirming the combined antibacterial and anti-inflammatory benefits of cefadroxil and curcumin. The fastest healing efficiency was due

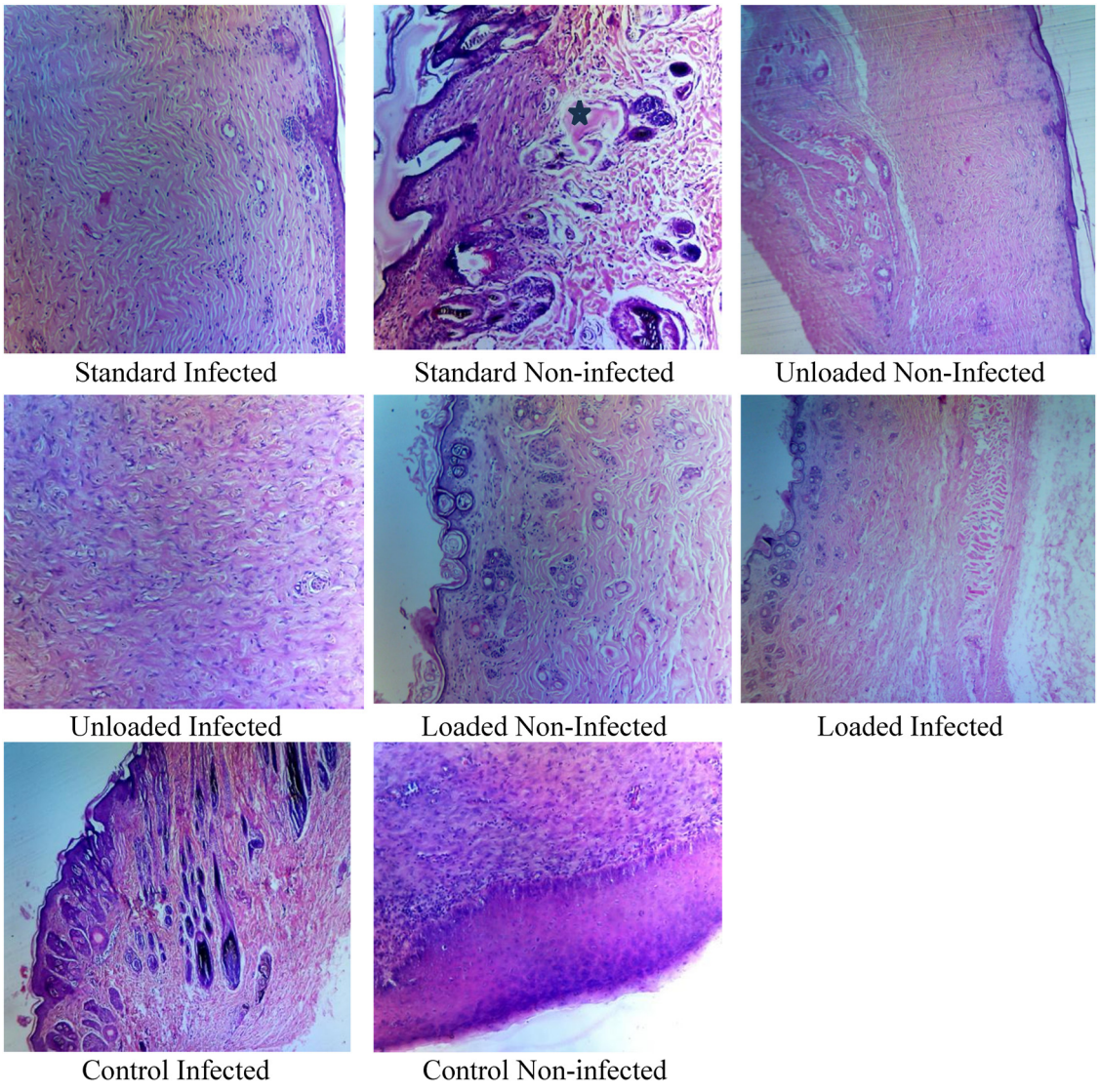

Figure 10: Histopathological investigations of healed tissues.

to the burst release of drugs from the formulations that killed bacteria at the wound site. The observed results were significantly different ($p < 0.05$). Antioxidant properties of PCL/CA/CeO2-CSNPs accelerated wound healing by inhibiting the formation of free radicals that could potentially enhance the chronicity of the wound [28]. The PVA/chitosan base nanocomposite film incorporated with mupirocin and cerium oxide exhibited an accelerated rate of wound healing [42]. Halarnekar et al. formulated zinc-oxide nanocomposites fused with chitosan and observed their wound-healing capacity. They observed the wound closure on the 15th day of treatment with a contraction of 95.67 ± 0.43%, compared to a control group with a contraction of 72.25 ± 0.64% [43] (Figure 9).

3.2.8 Histopathological investigations

Histopathological investigations were carried out to examine the effect of treatment on the wound healing process. Quantitative analysis showed CPCCNF-treated wounds had 35% higher collagen density and 1.8× greater epithelial thickness than untreated controls, confirming enhanced tissue regeneration. These findings provide objective evidence of CPCCNFs' superiority in wound healing. The nanofibers exhibited excellent results in the re-epithelization process, followed by decreased penetration of lymphocytes and neutrophils after 2 weeks of treatment compared to wounds covered with sterile gauze [28]. Hematoxylin and eosin-stained histological observations revealed that wounds treated with CPCCNFs had significantly ($p < 0.05$) increased epithelial growth and more compact collagen without necrosis and inflammation, as shown in Figure 10. Wounds treated with PVA-CS-CeNPs-MP showed lesser epidermal thickness [42,43], without scar formation [44,45], when stained with Masson's trichrome staining [46,47]. These findings are in accordance with the previous results [48,49].

4 Conclusion

Chitosan, PVA, cefadroxil, and curcumin-based nanofiber have been successfully formulated using the electrospinning technique. This combination leverages the additive impact of curcumin's biological features with cefadroxil's broad-spectrum antibacterial action, as indicated by the electrospun nanofiber system developed for wound healing. These findings indicate that the prepared nanofibers, especially the A4 formulation, exhibited the prerequisite features for wound healing application. The observed burst release followed by the sustained drug release pattern exhibits their efficacy in swift bacterial clearance and prolonged therapeutic action. Consequently, it is recommended that the fusion of these materials could be used in wound care products. Further studies are warranted in clinical settings in collaboration with wound healing providers.

Acknowledgments: We thank the Deanship of Ajman University, UAE for supporting the APC of this study. We acknowledge Khadija Amjad for improving the language of this manuscript.

Funding information: Authors state no funding involved.

Author contributions: Conceptualization: Saman Rashid, Muhammad Khurram Waqas, Ayesha Tahir, Haya Yasin, Bushra Nasir, Abida Kalsoom Khan, Munaza Ijaz, Ghulam Murtaza. Data curation: Saman Rashid, Ayesha Tahir, Munaza Ijaz, Ghulam Murtaza. Formal analysis: Saman Rashid, Ayesha Tahir, Abida Kalsoom Khan, Munaza Ijaz, Ghulam Murtaza. Funding acquisition: Haya Yasin, Ghulam Murtaza. Investigation: Saman Rashid, Ayesha Tahir, Abida Kalsoom Khan, Munaza Ijaz, Ghulam Murtaza. Methodology: Saman Rashid, Ayesha Tahir, Abida Kalsoom Khan, Munaza Ijaz, Ghulam Murtaza. Project administration: Ghulam Murtaza. Resources: Haya Yasin, Ghulam Murtaza. Software: Haya Yasin, Ghulam Murtaza. Supervision: Muhammad Khurram Waqas, Bushra Nasir, Ghulam Murtaza. Validation: Haya Yasin, Ghulam Murtaza. Visualization: Ghulam Murtaza. Writing – original draft: Saman Rashid, Muhammad Khurram Waqas, Ayesha Tahir, Haya Yasin, Bushra Nasir, Abida Kalsoom Khan, Munaza Ijaz, Ghulam Murtaza. Writing – review & editing: Ghulam Murtaza.

Conflict of interest: Authors state no conflict of interest.

Data availability statement: All data generated or analysed during this study are included in this published article.

References

[1] Wang H, Wang H, Ruan F, Feng Q, Wei Y, Fang J. High-porosity carbon nanofibers prepared from polyacrylonitrile blended with amylose starch for application in supercapacitors. Mater Chem Phys. 2023;293:126896.

[2] Wang K, Liu Y, Wang H, Liu Y, Yang X, Sun S. Multi-functional nanofilms capable of angiogenesis, near-infrared-triggered antibacterial activity and inflammatory regulation for infected wound healing. Biomater Adv. 2022;142:213154.

[3] Zhang J, Chen K, Ding C, Sun S, Zheng Y, Ding Q, et al. Fabrication of chitosan/PVP/dihydroquercetin nanocomposite film for in vitro and *in vivo* evaluation of wound healing. Int J Biol Macromol. 2022;206:591–604.
[4] Zhang L, Shi H, Tan X, Jiang Z, Wang P, Qin J. Ten-gram-scale mechanochemical synthesis of ternary lanthanum coordination polymers for antibacterial and antitumor activities. Front Chem. 2022;10:898324. doi: 10.3389/fchem.2022.898324.
[5] Dong X, Sun S, Wang X, Yu H, Dai K, Jiao J, et al. Structural characteristics and intestinal flora metabolism mediated immunoregulatory effects of Lactarius deliciosus polysaccharide. Int J Biol Macromol. 2024;278:135063. doi: 10.1016/j.ijbiomac.2024.135063.
[6] Ming T, Lei J, Peng Y, Wang M, Liang Y, Tang S, et al. Curcumin suppresses colorectal cancer by induction of ferroptosis via regulation of p53 and solute carrier family 7 member 11/glutathione/glutathione peroxidase 4 signaling axis. Phytother Res. 2024;38(8):3954–72. doi: 10.1002/ptr.8258.
[7] Sethuram L, Thomas JJB. Therapeutic applications of electrospun nanofibers impregnated with various biological macromolecules for effective wound healing strategy – A review. J Biomater Nanobiotechnol. 2023;157:113996.
[8] Gao T, Liao W, Lin L, Zhu Z, Lu M, Fu C, et al. Curcumae rhizoma and its major constituents against hepatobiliary disease: Pharmacotherapeutic properties and potential clinical applications. Phytomedicine. 2022;102:154090. doi: 10.1016/j.phymed.2022.154090.
[9] Lotfi Z, Khakbiz M, Davari N, Bonakdar S, Mohammadi J, Shokrgozar MA, et al. Fabrication and multiscale modeling of polycaprolactone/amniotic membrane electrospun nanofiber scaffolds for wound healing. Appl Organomet Chem. 2023;47(8):1267–84.
[10] Milner SM. Clinical perspectives on the use of allograft skin. ePlasty. 2024;24:QA16.
[11] Abbas M, Hussain T, Arshad M, Ansari AR. Wound healing potential of curcumin cross-linked chitosan/Polyvinylalcohol. Int J Biol Macromol. 2019;140:871–6. doi: 10.1016/j.ijbiomac.2019.08.153.
[12] Khunová V, Kováčová M, Olejniková P, Ondreáš F, Špitalský Z, Ghosal K, et al. Antibacterial electrospun polycaprolactone nanofibers reinforced by halloysite nanotubes for tissue engineering. Polymers. 2022;14(4):746. doi: 10.3390/polym14040746.
[13] Yang B, Yang H, Liang J, Chen J, Wang C, Wang Y, et al. A review on the screening methods for the discovery of natural antimicrobial peptides. J Pharm Anal. 2025;15(1):101046. doi: 10.1016/j.jpha.2024.101046.
[14] Zhang X, Wang Y, Gao Z, Mao X, Cheng J, Huang L, et al. Advances in wound dressing based on electrospinning nanofibers. J Am Pharm Sci. 2024;141(1):e54746.
[15] Saraiva MM, Campelo MdS, Camara Neto JF, Lima ABN, Silva GdA, Dias ATdFF, et al. Alginate/polyvinyl alcohol films for wound healing: Advantages and challenges. J Biomed Mater Res Part B: Appl Biomater. 2023;111(1):220–33.
[16] Mawazi SM, Kumar M, Ahmad N, Ge Y, Mahmood S. Recent applications of chitosan and its derivatives in antibacterial, anticancer, wound healing, and tissue engineering fields. J Polym. 2024;16(10):1351.
[17] Zia S, Khan SM, Butt MTZ, Gull NJ. Insight into CMC-PVA-fHNTs nanocomposite hydrogel as an advanced carrier for Cefadroxil Monohydrate: Fabrication and characterization/angiogenic potential analysis. Gels. 2024;10(4):235.
[18] Wang SH, Yuan HY, Li J, Pan SA, Xue X, Yue ZH, et al. Effect of electroacupuncture on NLRP3 inflammasome and morphology of the uterus in rats with primary dysmenorrhea based on meridian acupoint viscera correlation theory. World J Tradit Chin Med. 2023;9:123–30.
[19] Pang XB, Zhang XL, Wang MR, Yuan Y, Zhang X. Study on the effect of ginaton on reducing cerebral vasospasm and early brain injury after hemorrhagic stroke by inhibiting inflammatory response. World J Tradit Chin Med. 2024;10:33–9.
[20] Nguyen T-T, Vong LB, Ha NN-Y, Nguyen-Ngoc B-H, Doan HN, Dang NN-T, et al. Fabrication of electrospun polycaprolactone based membrane coated with curcumin chitosan nanoparticles and gelatin for wound dressing application. Mater Today Commun. 2024;40(1):110077.
[21] Xia TY, Wang Y, Yang YN, Wang WJ, Ding ZH, Zhong RX, et al. Extraction, purification, and anti-inflammatory activity of steroid fraction from Physalis alkekengi L. Var. Franchetii (Mast.) Makino. World J Tradit Chin Med. 2023;9:167–77.
[22] Xu HJ, Yang Y, Dong YQ, Niu KM, Li TY, Deng H, et al. Anti-inflammatory effect of Dendrobium huoshanense polysaccharides on carrageenan-induced air pouch synovitis in mice. World J Tradit Chin Med. 2023;9:399–403.
[23] Ahmed Naseem M, Hussain Z, Thu HE, Khan S, Sohail M, Sarfraz RM, et al. Nanotechnology-mediated developments for improving physicochemical properties and wound healing efficacy of curcumin: A review. Int J Polym Mater Polym Biomater. 2024;74(5):1–20. doi: 10.1080/00914037.2024.2342908.
[24] Dutta J, Devi N. Preparation, optimization, and characterization of chitosan-sepiolite nanocomposite films for wound healing. Int J Biol Macromol. 2021;186:244–54.
[25] Govindasamy GA, Mydin SMN, Gadaime NKR, Sreekantan S. Phytochemicals, biodegradation, cytocompatibility, and wound healing profiles of chitosan film embedded with green synthesized antibacterial ZnO/CuO nanocomposite. J Polym Environ. 2023;31(10):4393–409.
[26] Chang R, Zhao D, Zhang C, Liu K, He Y, Guan F, et al. Nanocomposite multifunctional hyaluronic acid hydrogel with photothermal antibacterial and antioxidant properties for infected wound healing. Int J Biol Macromol. 2023;226:870–84. doi: 10.1016/j.ijbiomac.2023.02.157.
[27] Wang Y, Ding C, Zhao Y, Zhang J, Ding Q, Zhang S, et al. Sodium alginate/poly(vinyl alcohol)/taxifolin nanofiber mat promoting diabetic wound healing by modulating the inflammatory response, angiogenesis, and skin flora. Int J Biol Macromol. 2023;252:126530.
[28] Kamalipooya S, Fahimirad S, Abtahi H, Golmohammadi M, Satari M, Dadashpour M, et al. Diabetic wound healing function of PCL/cellulose acetate nanofiber engineered with chitosan/cerium oxide nanoparticles. Int J Pharm. 2024;653:123880.
[29] Wang Y, Xu Y, Zhai W, Zhang Z, Liu Y, Cheng S, et al. In-situ growth of robust superlubricated nano-skin on electrospun nanofibers for post-operative adhesion prevention. Nat Commun. 2022;13(1):5056. doi: 10.1038/s41467-022-32804-0.
[30] Basha M, AbouSamra MM, Awad GA, Mansy SS. A potential antibacterial wound dressing of cefadroxil chitosan nanoparticles in situ gel: Fabrication, in vitro optimization and *in vivo* evaluation. Int J Pharm. 2018;544(1):129–40. doi: 10.1016/j.ijpharm.2018.04.021.
[31] Iqbal H, Khan BA, Khan ZU, Razzaq A, Khan NU, Menaa B, et al. Fabrication, physical characterizations, and in vitro antibacterial activity of cefadroxil-loaded chitosan/poly(vinyl alcohol) nanofibers

against Staphylococcus aureus clinical isolates. Int J Biol Macromol. 2020;144:921–31.
[32] Idumah CI, Okonkwo U, Obele CJ. Recently emerging advancements in montmorillonite polymeric nanoarchitectures and applications. Curr Mater. 2022;4:100071.
[33] Gao C, Zhang L, Wang J, Jin M, Tang Q, Chen Z, et al. Electrospun nanofibers promote wound healing: Theories, techniques, and perspectives. J Nanomater. 2021;14:3106–30.
[34] Wu T, Fu Y, Guo S, Shi Y, Zhang Y, Fan Z, et al. Self-assembly multifunctional DNA tetrahedron for efficient elimination of antibiotic-resistant bacteria. Aggregate. 2024;5(1):e402. doi: 10.1002/agt2.402.
[35] Ghosal K, Agatemor C, Špitálsky Z, Thomas, Kny E. Electrospinning tissue engineering and wound dressing scaffolds from polymer-titanium dioxide nanocomposites. Chem Eng J. 2019;358:1262–78. doi: 10.1016/j.cej.2018.10.117.
[36] Ghosal K, Kováčová M, Humpolíček P, Vajďák J, Bodík M, Špitalský Z. Antibacterial photodynamic activity of hydrophobic carbon quantum dots and polycaprolactone based nanocomposite processed via both electrospinning and solvent casting method. Photodiagn Photodyn Ther. 2021;35:102455. doi: 10.1016/j.pdpdt.2021.102455.
[37] Pandey VK, Ajmal G, Upadhyay SN, Mishra PK. Nano-fibrous scaffold with curcumin for anti-scar wound healing. Int J Pharm. 2020;589:119858.
[38] Barman M, Mahmood S, Augustine R, Hasan A, Thomas S, Ghosal K. Natural halloysite nanotubes/chitosan based bio-nanocomposite for delivering norfloxacin, an anti-microbial agent in sustained release manner. Int J Biol Macromol. 2020;162:1849–61. doi: 10.1016/j.ijbiomac.2020.08.060.
[39] Massoumi B, Sarvari R, Fakhri E, Emami Rad K. Conductive nanofibrous scaffold based on polyvinyl alcohol/cellulose nanocrystals/reduced graphene oxide composite reinforced with curcumin for wound healing. J Ultrafine Grained Nanostruct Mater. 2024;57(1):92–103.
[40] Merlusca IP, Matiut DS, Lisa G, Silion M, Gradinaru L, Opera S, et al. Preparation and characterization of chitosan-poly(vinyl alcohol)-neomycin sulfate film. Polym Bull. 2018;75(9):3971–86.
[41] Rezagholizade-Shirvan A, Najafi MF, Behmadi H, Masrournia MJ. Preparation of nano-composites based on curcumin/chitosan-PVA-alginate to improve stability, antioxidant, antibacterial and anticancer activity of curcumin. Int J Biol Macromol. 2022;145:110022.
[42] Liu H, Chen R, Wang P, Fu J, Tang Z, Xie J, et al. Electrospun polyvinyl alcohol-chitosan dressing stimulates infected diabetic wound healing with combined reactive oxygen species scavenging and antibacterial abilities. Carbohydr Polym. 2023;316:121050.
[43] Halarnekar D, Ayyanar M, Gangapriya P, Kalaskar M, Redasani V, Gurav N, et al. Eco synthesized chitosan/zinc oxide nanocomposites as the next generation of nano-delivery for antibacterial, antioxidant, antidiabetic potential, and chronic wound repair. Int J Biol Macromol. 2023;242:124764.
[44] Chen S, Tian H, Mao J, Ma F, Zhang M, Chen F, et al. Preparation and application of chitosan-based medical electrospun nanofibers. Int J Biol Macromol. 2023;226:410–22.
[45] Chen K, Hu H, Zeng Y, Pan H, Wang S, Zhang Y, et al. Recent advances in electrospun nanofibers for wound dressing. Eur Polym J. 2022;178:111490.
[46] Loo HL, Goh BH, Lee LH, Chuah LH. Application of chitosan-based nanoparticles in skin wound healing. Asian J Pharm Sci. 2022;17(3):299–332.
[47] Tan SM, Teoh XY, Hwang JL, Khong P, Sejare R, Almashhadani AQ, et al. Electrospinning and its potential in fabricating pharmaceutical dosage forms. J Drug Delivery Sci Technol. 2022;76:103761.
[48] Wang Y, Zhai W, Li J, Liu H, Li C, Li J. Friction behavior of biodegradable electrospun polyester nanofibrous membranes. Tribol Int. 2023;188:108891. doi: 10.1016/j.triboint.2023.108891.
[49] Zheng Q, Zhang W, Wang L, Wen X, Wu J, Ren Y, et al. Functional dyeing of cellulose macromolecule/synthetic fibers two-component fabrics with sustainable microbial prodigiosins. Int J Biol Macromol. 2024;278:134964. doi: 10.1016/j.ijbiomac.2024.134964.